Eng. Sci., 2022, **17**, 216–223

Engineered Science

DOI: https://dx.doi.org/10.30919/es8d517

Nickel Oxide Embedded with Polymer Electrolyte as Efficient Hole Transport Material for Perovskite Solar Cell

Monika Srivastava, Karan Surana, Pramod Kumar Singh and Ram Chandra Singh*

Abstract

The use of organic hole transport material (HTM) is usually quite expensive owing to its synthesis procedure and high purity requirement. Therefore, we have synthesized an inexpensive, inorganic HTM, nickel oxide (NiO). The perovskite precursor *i.e.*, CH_3NH_3I were also synthesized and characterized for surface morphology and elemental analysis. Perovskite solar cell (PSC) was successfully prepared using NiO as the HTM with a supporting layer of polymer electrolyte. The fabricated sandwich-structured PSC exhibited an open circuit voltage (V_{oc}) of 0.77 V, short circuit density (J_{sc}) of 18 mA/cm^2, and an effective photon conversion efficiency (PCE) of 5.13%.

Keywords: Perovskite; Polymer electrolyte; Nickel oxide; Perovskite solar cell; Hole transport material.
Received: 14 June 2021; Revised: 23 August 2021; Accepted: 30 August 2021.
Article type: Research article.

1. Introduction

Perovskite solar cells (PSCs) based on methyl ammonium lead halide (CH_3NH_3PbX; X = halide) are one of the most promising candidates for efficient and cost-effective use of solar energy in the field of photovoltaics. The power conversion efficiency (PCE) has increased rapidly from 3.8% to ~24% in only ten years. Among the initial reports by Kojima *et al*., they worked on two types of PSCs, viz., $CH_3NH_3PbI_3$ and $CH_3NH_3BrI_3$, and achieved a PCE of 3.8% and 6.5%, respectively.[1] These breakthroughs suggested that the coming years will advance the perovskite-based solar cells to a higher efficiency while retaining low cost and easy processability.[2] In another report, PCE of over 18% was obtained by replacing TiO_2 with SnO_2. It further stated that for large-scale manufacturing, the planar electron selective layers are more suitable than the mesoporous ones.[3] Another study suggested that the fabrication of a very thin perovskite layer is crucial for high-performance PSCs. PCE of 22.1% for smaller cells and 19.7% for 1 cm^2 cell were achieved.[4]

Perovskites have many useful properties like the ease of processing, band tunability, and high absorption coefficient, which help in achieving better photovoltaic characteristics in PSCs. On the other hand, the hole transport material (HTM) also plays an important role as it is responsible for effective charge extraction and collection at the electrodes. Many studies have reported the use of organic HTMs like Spiro–MeOTAD, but it is neither cost-effective nor viable for the large-scale production of solar cells.[5] There is a wide range of inorganic–type semiconductors, which can play the role of HTM for the effective fabrication of PSCs, such as CuSCN, Cu_2O, CuO, CuI, or NiO_x. The use of CuSCN results in thermally stable PSCs, which retain even better operational stability if GO (graphene oxide) is applied in between the CuSCN and Au contact. PSCs using CuI as HTM succeeded in achieving a PCE of 6.0% with a stable photocurrent.[6,7] A CuO_x hole transport layer (HTL) was used by Sun *et al*. in an inverted planar heterojunction PSC, which resulted in a PCE of 17.1%, an open circuit voltage (V_{oc}) of 0.99 V, a short–circuit current density (J_{sc}) of 23.2 mA·cm^{-2}, and a fill factor (FF) of 74%. The use of Cu_2O resulted in a PCE of 13.35%, making it one of the most promising HTMs in the field of photovoltaics.[8,9]

The fabrication of PSC with NiO, ap–type inorganic semiconductor, as the HTM has also been reported. It was observed that PSC with NiO as HTM not only showed good efficiency but it also helped in increasing the V_{oc} to over 1 V.[10] NiO has good optical transparency, reduces electron leakage, and has suitable energy levels to possess a wide band gap, which makes it a promising candidate as HTM for PSC.[11,12] It also acts as an electron-blocking layer, suppressing charge recombination, thereby facilitating a better charge (hole) extraction in solar cells. Jeng *et al*. obtained the highest PCE of 15.2% using NiO_x where the NiO_x film was sputter coated

Center of Excellence on Solar Cells & Renewable Energy, Department of Physics, School of Basic Sciences and Research, Sharda University, Greater Noida, U.P. 201310, India.
**E–mail:* rcsingh@sharda.ac.in (R.C. Singh)

over the perovskite layer.[13] NiO has a favorable deep–lying highest occupied molecular orbital (HOMO, valence band edge value) with the work function between 5 and 5.6 eV.[14] Regarding the effect of NiO on fluorine-doped tin oxide (FTO), it was reported that being an inert material, NiO is non–corrosive towards FTO substrates.[15] Initially, Snaith *et al*. used the NiO layer as HTM and obtained a low PCE of < 0.1%, which was due to improper contact between the perovskite and NiO layer.[2] An efficient inverted planar PSC was fabricated where NiO was used as the hole–collecting layer and the irradiation with UV light helped to increase its work function.[16] Liu *et al*. deposited $CH_3NH_3PbI_3$ onto the NiO layer through spin–coating and fabricated a planar ITO/NiO/$CH_3NH_3PbI_3$/PCBM/BCP/Al (where ITO is Indium tin oxide, PCBM is Phenyl-C61-butyric acid methyl ester and BCP is bathocuproine) device, which exhibited an efficiency of 7.9%; however, when a mesoporous NiO layer was used, the efficiency was increased to 9.51%.[17] They also found that the ultraviolet–ozone (UVO) treatment was beneficial for the device. In another study, NiO/$CH_3NH_3PbI_3$ solar–cell device was used and the rough NiO film surface caused the formation of an intimate, large interfacial–area junction with the $CH_3NH_3PbI_3$ film, which dramatically improved the cell efficiency.[18,19] These results in general portray that NiO is indeed a very promising functional HTL in PSCs. In the recent reports of PSCs with NiO as HTM, a record efficiency of 22.1% had been reported with a hybrid organic-inorganic perovskite material. However, NiO is reactive towards perovskite under the effect of light, temperature, and electrical stress, which is detrimental to the long–term stability of PSC.[20] In another study, the $CH_3NH_3PbI_{3-x}Cl_x$ has been used with NiO HTM leading to the development of a highly stable interface maintaining 85% efficiency after 670 h.[21] Alternatively, KI-modified NiO was used as HTM in inverted PSCs, which improved the photovoltaic parameters by increasing the FF to 0.814.[22] Another comparative study of PSCs between PEDOT: PSS and Cu-doped NiO as HTM showed that in addition to enhanced photovoltaic performance, the latter also showed a slower degradation.[23]

In the present work, we report the synthesis of perovskite ($CH_3NH_3PbI_3$) material in ambient conditions. The synthesis of NiO was carried out using a simple sol-gel method. The prepared materials were further characterized for UV–Vis absorption,x–ray diffraction (XRD), energy dispersive–ray (EDX), and scanning electron microscopy (SEM). The prepared sandwich structured PSC with a supporting layer of polymer electrolyte resulted in a V_{oc} of 0.77 V, J_{sc} of 18 mA·cm^{-2}, and PCE of 5.13% in an ambient condition.

2. Experimental section

The materials used for synthesis are given in the supplementary information.

2.1 Preparation of methyl ammonium iodide (MAI)

The perovskite precursor, methyl ammonium iodide (CH_3NH_3I), was synthesized by mixing 27.86 mL of methylamine (CH_3NH_2) and 30 mL of HI in a round bottom flask kept under ice–bath treatment at 0 ºC for 2 h. The obtained product was kept in a laboratory oven at 60 ºC for 24 h, which resulted in a light–yellow-colored precipitate. The precipitate was then washed thoroughly with diethyl ether resulting in whitish crystals. Further, the precipitate was kept at 100 ºC in a vacuum oven for 24 h to obtain dried powders. For the synthesis of the $CH_3NH_3PbI_3$ solution, the prepared CH_3NH_3I powder was mixed with PbI_2 in 2 mL of dimethylformamide (DMF) in an equal ratio. The solution was stirred continuously for approximately 6 h at 60 °C which resulted in the formation of methyl ammonium lead iodide ($CH_3NH_3PbI_3$ or $MAPbI_3$) perovskite solution.[24]

2.2 Synthesis of NiO

NiO powder was prepared by mixing 1.5 g of $NiCl_2{\cdot}6H_2O$ with 70 mL ethanol under continuous stirring. In another beaker, 0.5 g NaOH was dissolved in 100 mL ethanol. Both the solutions were continuously stirred for approximately 2 h, which resulted in the formation of a light–green colored gel. The gel was kept undisturbed for three hours, following which it was filtered and washed with double distilled (DD) water and ethanol, leaving behind light–a green-colored precipitate. The precipitate was dried in an oven at 100 °C for 2 h, which resulted in the formation of fine green powder as shown in the supplementary information (Fig. S1).[25]

2.3 Preparation of polymer electrolyte

The polymer electrolyte solution consisting of polyethylene oxide (PEO) with 10% KI and 1% I_2 was prepared in 20 mL acetonitrile. In a typical process, the solution was kept on a magnetic stirrer for a few days to allow uniform mixing and sufficient evaporation of the solvent. The obtained quasi-solid electrolyte was used in the sandwich-structured perovskite solar cells.[26]

2.4 Fabrication of the perovskite solar cells

The preparation of working and counter electrodes is crucial, as they are responsible for the proper functioning of the solar cells. Firstly, the FTO glasses were sonicated thoroughly in DD water followed by acetone. For the preparation of the working electrode (WE), the blocking layer (BL) was spin-coated at ~1000 rpm for 60 s and then kept for calcination at 500 °C for 30 min in a furnace. The thickness of the TiO_2 film was optimized by using two layers of scotch adhesive tapes. The TiO_2 paste was spread by the doctor blade method on the BL-coated FTO and calcined at 500 ºC for 30 min resulting in a TiO_2 film of a thickness ~of 10 µm.[27] The counter electrode (CE) was prepared by spin-coating of H_2PtCl_6 solution on an FTO glass followed by calcination at 500 °C for 30 min.

The prepared perovskite solution was spin-coated on the TiO_2 layer followed by heating at 70 °C for 30 min on a hot plate.[28,29] For the preparation of HTM, 0.72 g of green-colored NiO powder was mixed with 2 mL of 6% HCl and subjected

to constant stirring at 90 °C for 10 min.[30] After spin coating at a speed of ~1500 rpm for 60 s, the substrate was heated at 100 °C for 10 min.[31,32] A thin layer of PEO polymer electrolyte was coated over the NiO film. The Pt CE has finally been sandwiched over the electrolyte-coated WE. The final architecture of the prepared PSC was FTO/BL/TiO_2/Perovskite/NiO/PEO/Pt/FTO.

3. Results and discussion

The details of characterization techniques used are given in supplementary information.

3.1 Scanning electron microscopy (SEM)

Figure 1 demonstrates the SEM image of $MAPbI_3$ film, which depicts islands of well–defined flowery rod-like structures illustrating the crystalline nature of the sample. The rod-shaped structures of $MAPbI_3$ are favorable for efficient charge transfer applications and act as better light harvesters as these rods not only absorb a portion of the wave incident directly on it but also the surrounding ones.[33-35] On further magnification, it is observed that these rods have a porous surface, which allows the HTM solution to properly seep into the perovskite layer, thus creating a better interface for charge transfer through the HTM.

Figure 2 illustrates the surface morphology of NiO, whereby the presence of non-uniform particles of different sizes can be observed (Fig. 2(a)). Further magnification (Figs. 2(b) and (c)) reveals the agglomeration of particles with distinctly visible cracks. The agglomeration of particles tends to the formation of granules, which challenges the uniform deposition of the NiO solution on the perovskite layer. Consequently, this affects the formation of a proper interface between perovskite and NiO.

3.2 Atomic force microscopy (AFM)

The subsequent layers of the WE may have varying surface roughness as well as porosity. The surface roughness of any layer is determined by the R_{rms} value, *i.e.*, the root means the square value of roughness. R_{rms} are obtained by the standard deviation of data from AFM images. The formula for R_{rms} is given by Equation (1):

$$R_{rms} = \sqrt{\frac{\sum_{n=1}^{N}(z_n - \bar{z})^2}{N-1}} \quad (1)$$

where z_n is the height of the n^{th} AFM data and $\bar{z}$ represents the mean value of z_n of the AFM images, while N represents the number of AFM data. In this study, all the measurements have been performed over films coated on the FTO substrate.

Figures 3 and 4 represent the 3D AFM images of FTO coated with TiO_2 and FTO coated with TiO_2/perovskite layer, respectively. Figs. 3(a) and 3(b) show a wide range of high-intensity peaks and also the highly porous nature of the TiO_2 layer. When the $MAPbI_3$ layer is spin coated on TiO_2 (Fig. 4), the surface roughness decreases from 13.9 to 10.7 nm, which suggests the proper coverage of perovskite material over the TiO_2 surface. A reduction in the high-intensity peaks is also seen in Fig. 4. Further, the pores (black regions) in TiO_2 (Fig. 3b) almost vanished upon perovskite coating (Fig. 4b). Thus, the study of variation in the surface morphology of TiO_2 and the perovskite layer in terms of roughness also concludes that perovskite is properly adsorbed onto the TiO_2 layer.

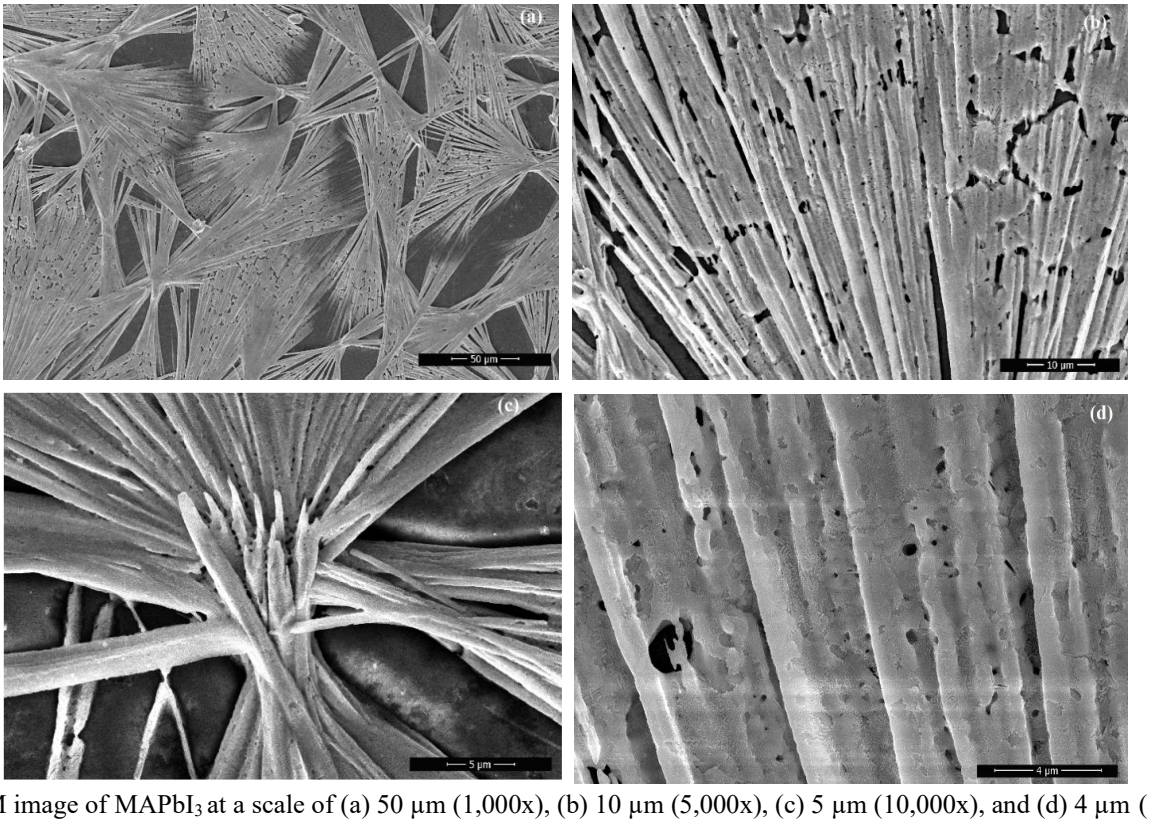

Fig. 1 SEM image of $MAPbI_3$ at a scale of (a) 50 µm (1,000x), (b) 10 µm (5,000x), (c) 5 µm (10,000x), and (d) 4 µm (10,000x).

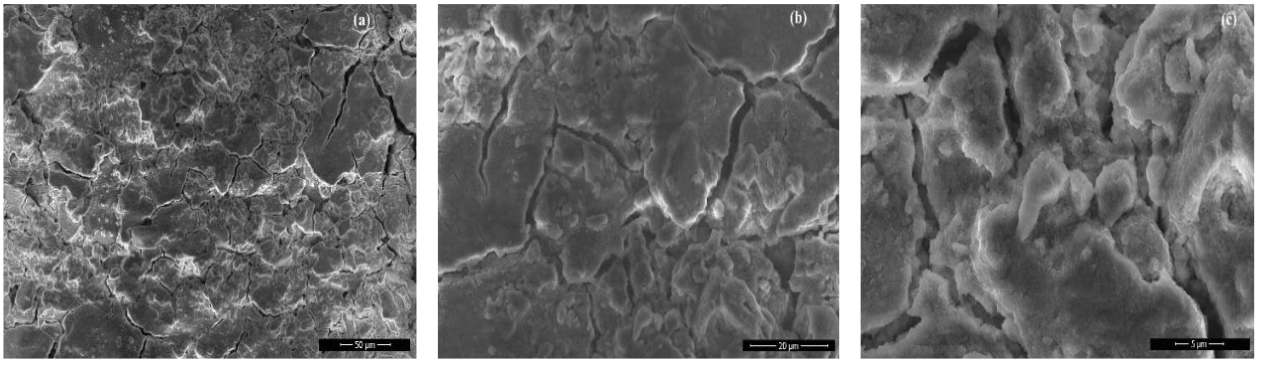

Fig. 2 SEM images of NiO at a scale of (a) 50 µm (1,000x), (b) 20 µm (4,000x), and (c) 5 µm (10,000x), respectively.

3.3 Energy dispersive X-ray (EDX)

The EDX microanalysis technique determines the elemental composition of a compound by electron microscopy based on the generation of characteristic x–rays. As a result, it also helps to analyze the purity of a synthesized sample or compound. The elemental analysis of the synthesized perovskite is depicted in Fig. S2 (supplementary information), which clearly shows the absence of any foreign elements, thereby affirming the purity of the prepared material. The atomic weight percentage of the elements is given in Table 1.

Table 1. Elemental composition of $MAPbI_3$ in weight %.

Element	At. No.	Series	Norm. C [wt.%]	Atom. C [at%]
Pb	82	M-series	53.77	33.32
I	53	L-series	44.06	44.57
C	6	K-series	1.49	15.92
N	7	K-series	0.67	6.18
			100.00	100.00

Table 2. Elemental composition of Nickel Oxide in weight %.

Element	At. No.	Series	Norm. C [wt.%]	Atom. C [at%]
Ni	28	K-series	78.73	48.26
O	8	K-series	16.05	36.09
C	6	K-series	5.22	15.65
			100.00	100.00

Figure S3 (supplementary information) shows the presence of elements nickel (Ni) and oxygen (O) with the atomic weight percent as given in Table 2. This confirms that the sol-gel method used for the preparation of NiO is effective. A small percentage of impurity in the form of carbon is also present, which could have appeared during the sample loading.

3.4. X-ray diffraction (XRD) studies

The obtained XRD pattern of $MAPbI_3$ is depicted in Fig. 5. The crystallite size was calculated by using Debye-Scherrer's formula, which is given by Equation (2):

$$D = k\lambda/\beta Cos\theta \quad (2)$$

where k is an empirical constant equal to 0.9, λ is the wavelength of the x-ray source = 1.5405 Å, β is the full width at half maximum (FWHM) of the diffraction peak, and θ is the angular position of the peak. The calculated crystallite size from the XRD pattern is 45.82 nm, which indicates the formation of $MAPbI_3$ nanoparticles. The XRD pattern of the perovskite material shows peaks at 13.26°, 20.56°, 29.03°, 32.45°, 39.25°, 41.02°, and 52.91° which are in close agreement with the reported peaks.[36] The 2θ values correspond to (100), (110), (200), (210), (310), (330), and (004), respectively, which is indicative of cubic structured $MAPbI_3$. However, it also suggests the phase transition of perovskite material from tetragonal to cubic crystal structure which occurs at ~ 67 °C.[37] The hump from 20° to 35° along with the unmarked peaks are attributed to the presence of amorphous SiO_2 (glass slide).[38]

The XRD pattern of powdered NiO is presented in Fig. 6. As observed, three major peaks are observed at 2θ = 38°, 43°, and 62° which is in good agreement with the JCPDS data

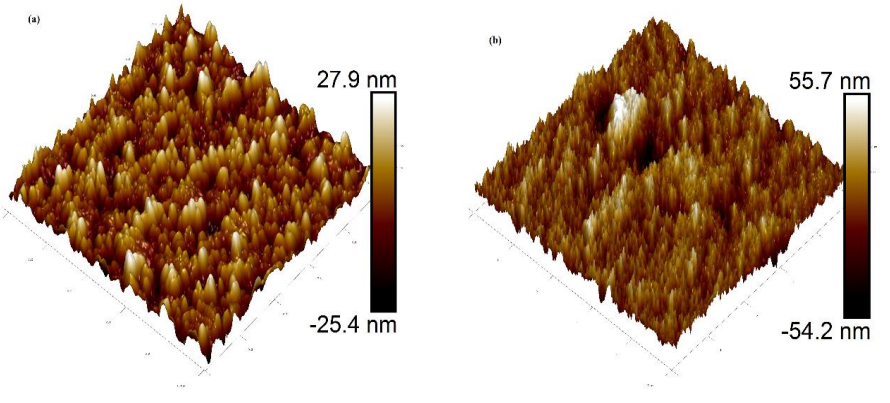

Fig. 3 3D AFM image of TiO_2 at an average width of (a) 1 µm and (b) 5 µm.

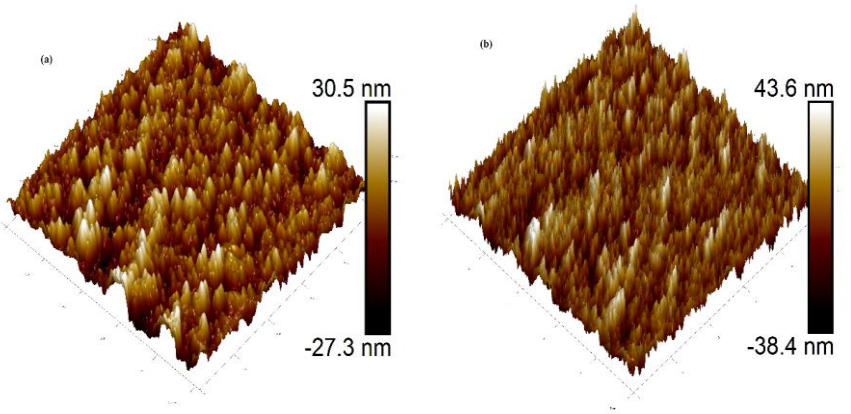

Fig. 4 3D AFM image of perovskite layer at an average width of (a) 1 μm and (b) 5 μm.

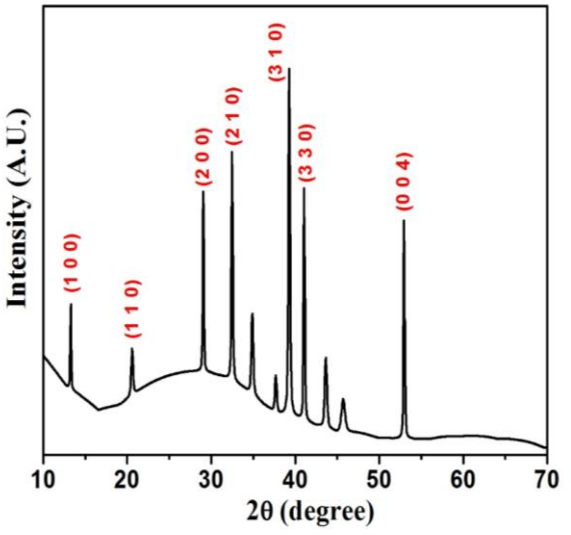

Fig. 5 XRD pattern of $MAPbI_3$.

(JCPDS card No. 22–1189).[39] The corresponding miller indices for the aforementioned peaks are (1 1 1), (2 0 0), and (2 2 0), respectively.[39,40] The obtained pattern is further indicative of the crystalline nature of the HTM.[41]

3.5 SEM analysis of PSC

Figure 7(a) represents the porous TiO_2 coating on FTO. Owing to the mesoporous nature of TiO_2, the pores are not visible in the SEM image. From Fig. 7(b), it is clear that the surface morphology changes upon spin coating of perovskite onto TiO_2. Tiny island-type structures of perovskite can be seen in the image, which resembles the SEM image of only perovskite material (Fig. 1), thereby further confirming that perovskite has covered the TiO_2 in its entirety. The rod-type structure formation should help in better trapping of photons as well as facilitate an efficient charge transfer. The perovskite layer is followed by drop–casting the NiO solution. From the SEM analysis of the NiO layer (Fig. 7(c)), it is clear that it consists of highly aggregated spherical particles, which offers a better surface area. Further, it can be observed that NiO covers the perovskite layer perfectly with minute cracks.

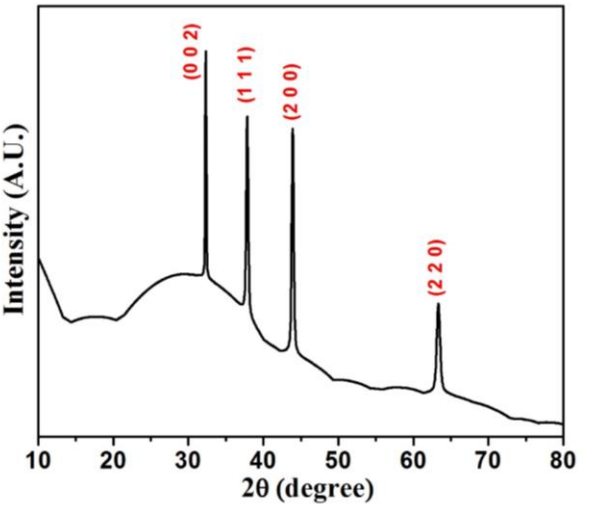

Fig. 6 XRD of NiO powder.

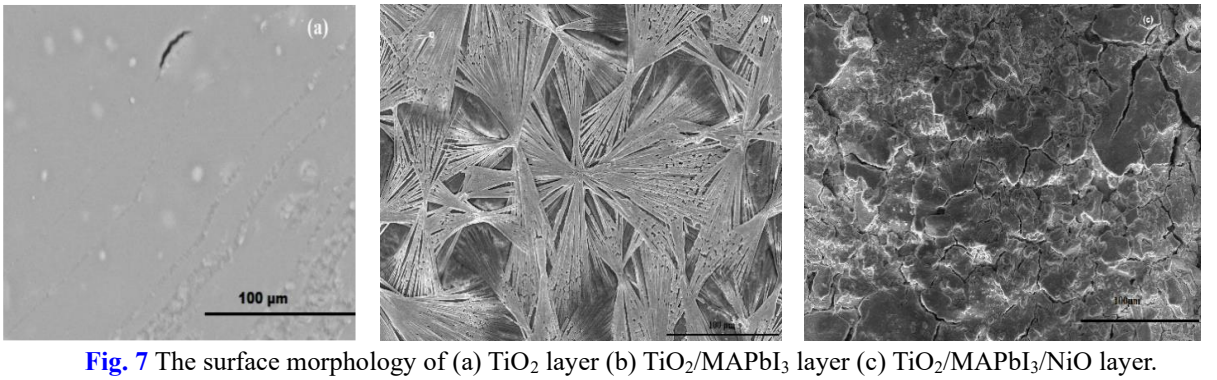

Fig. 7 The surface morphology of (a) TiO_2 layer (b) $TiO_2/MAPbI_3$ layer (c) $TiO_2/MAPbI_3/NiO$ layer.

The cross-sectional view of the WE of the fabricated PSC is shown in Fig. 8. This image represents the successful fabrication of different layers of PSC, *i.e.*, TiO_2 which acts as electron transport layer (ETL), perovskite as the sensitizer, and NiO playing the role of HTL, thus achieving a well-formed hetero–junction structure of PSC. However, it should be noted that apart from the TiO_2 layer, the thicknesses of perovskite and NiO are much greater than the optimum one. For instance, the reported ideal thickness for the perovskite layer is 200 – 400 nm and that of the HTL is < 180 nm.[42,43] Since, no sophisticated tools were used, controlling the thickness of the sensitizer and NiO deposition was not possible.

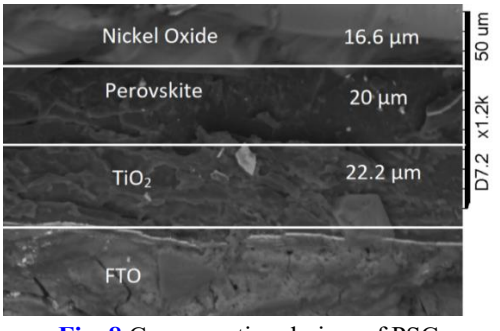

Fig. 8 Cross–sectional view of PSC.

3.6 Photovoltaic performance

The obtained characteristic of the PSC with an active area of 0.40 cm^2 is shown in Fig. 9. An above-average V_{oc} of 0.77 V was obtained with a decently high J_{sc} of 18 mA/cm^2. However, the J–V curve did not have the ideal rectangular shape, hence a low FF of 0.37 was obtained. The low value of FF indicates the non-uniform formation of different semiconductor layers, high interface impedance (as observed in the impedance curve, Fig. 11), and recombination losses. The non-uniform formation of the functional layers is attributed to the use of the spin-coating technique, which although is cost-effective but probably not suitable for PSC. The calculated PCE in ambient conditions was 5.13%.

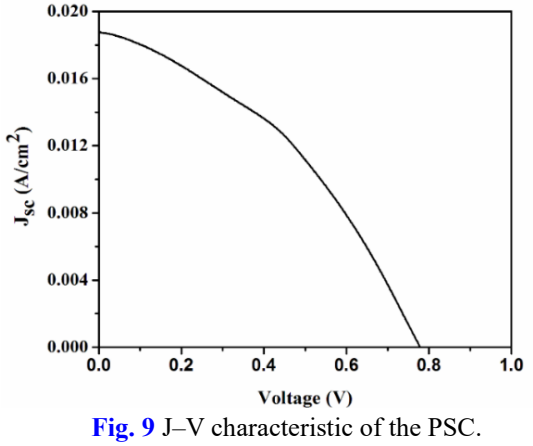

Fig. 9 J–V characteristic of the PSC.

The absorption of photons in the active layer of perovskite leads to the generation of electron-hole pairs. The excited electrons move to the conduction band (CB) of TiO_2 leaving behind a hole in the valence band (VB) of the perovskite. The Fermi level of TiO_2 increases as the excited electrons from the CB of $MAPbI_3$ moves to the CB of TiO_2 while the hole moves towards the VB of NiO (HTM), which is a wideband gap material. The CB of NiO lies at approximately −2.2 eV, which is much higher than the CB of $MAPbI_3$, *i.e.*, -3.9 eV.[44] Therefore, the injection of electrons from the CB of $MAPbI_3$ into the CB of NiO is not energetically favorable, which suggests that HTM also acts as an electron-blocking layer.[45] The addition of polymer electrolyte after the HTM layer improves the contact between the sandwiched electrodes, thereby helping the efficient charge transfer through the redox couple (I_3^-/I^-). The redox couple acts as a shuttle to carry the electrons, thus regenerating the HTM as well as the perovskite sensitizer. The schematic diagram of the entire process with energy band levels as given in the literature is shown in Fig. 10.

As evident from the previous results, the use of only polymer electrolytes leads to poor efficiency (0.9%).[26] However, with the addition of NiO as HTM between the electrolyte and perovskite, the characteristics improve drastically. This is evident from the rise in efficiency to 5.13% from 0.9%.

3.7 Impedance spectroscopy

The obtained impedance graph was subjected to curve fitting (Fig. 11) where R_s is the series resistance comprising of the wires, FTOs, and clips; R_t is the resistance at the junction between WE (blocking layer to dye) and electrolyte while R_c is the resistance at the junction between electrolyte and CE.[46] The equivalent circuit is shown in the inset of Fig. 11.

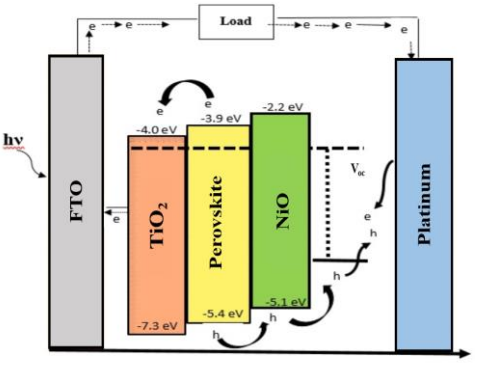

Fig. 10 Schematic diagram of the charge transfer process in a PSC.

The inset of Fig. 11 also presents the expanded initial region of impedance where the initial high-frequency impedance is shifted from zero. This shift of 18 Ω accounts for the value of R_s. The first partially formed semi-circle gives the value of R_c which stands at 24.36 Ω. The low value of junction resistance between electrolyte and CE suggests a smooth interface between these two. The value of R_t is rather high, i.e., 2211.26 Ω, which is expected owing to the use of the polymer electrolyte.[46,47] Nevertheless, the well-formed impedance pattern of the PSC shows the proper junction formation and smooth charge transfer between the individual components.

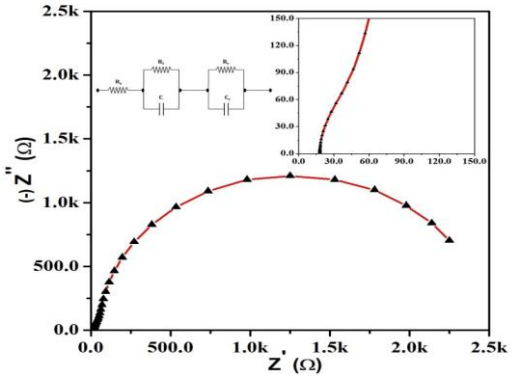

Fig. 11 Impedance analysis of the PSC under 1 sun condition. (Inset) Expanded initial region and equivalent circuit.

4. Conclusions

The present work was focused on the fabrication of PSC in a sandwich configuration using NiO as HTM embedded with polymer electrolyte in an ambient condition. The rod-type structured perovskite enabled efficient trapping of photons and generated a decent photocurrent. The NiO well served its role of being an efficient inorganic HTM by transporting the holes to the CE via the polymer electrolyte while also suppressing the electron recombination. The simple sandwich architecture of the PSC led to a V_{oc} of 0.77 V, a J_{sc} of 18 mA/cm^2 with an overall PCE of 5.13%. However, the obtained efficiency is low as compared to the ones mentioned in the literature, which is chiefly attributed to the preparation of PSC at ambient conditions, the use of polymer electrolyte, and the utilization of low–cost techniques, such as spin–coating and doctor blading. The fabrication of PSC in laboratory ambient conditions reflects upon its low cost and its easily processable nature. The low value of FF suggests the modification in the architecture of the PSC, possibly in the context of a suitable polymer electrolyte which would also help in lowering the junction resistance, thereby improving the overall photovoltaic characteristics. The studies of PSC using only NiO and other HTMs are underway.

Acknowledgments

The author KS is thankful to CSIR, India for providing the Senior Research Fellowship (SRF, 9/1078(0002)/18 EMR–I).

Conflict of interest

There are no conflicts to declare.

Supporting information

Applicable.

References

[1] A. Kojima, K. Teshima, Y. Shirai, T. Miyasaka, *Journal of the American Chemical Society*, 2009, **131**, 6050-6051, doi: 10.1021/ja809598r.

[2] H. J. Snaith, *The Journal of Physical Chemistry Letters*, 2013, **4**, 3623-3630, doi: 10.1021/jz4020162.

[3] J. P. Correa-Baena, A. Abate, M. Saliba, W. Tress, T. Jesper Jacobsson, M. Grätzel, A. Hagfeldt, *Energy & Environmental Science*, 2017, **10**, 710-727, doi: 10.1039/c6ee03397k.

[4] W. S. Yang, B.-W. Park, E. H. Jung, N. J. Jeon, Y. C. Kim, D. U. Lee, S. S. Shin, J. Seo, E. K. Kim, J. H. Noh, S. I. Seok, *Science*, 2017, **356**, 1376-1379, doi: 10.1126/science.aan2301.

[5] M. Liu, M. B. Johnston, H. J. Snaith, *Nature*, 2013, **501**, 395-398, doi: 10.1038/nature12509.

[6] N. Arora, M.I. Dar, A. Hinderhofer, N. Pellet, F. Schreiber, S. M. Zakeeruddin, M. Grätzel, *Science*, 2017, **358**, 768-771, doi: 10.1126/science.aam5655.

[7] J. A. Christians, R. C. M. Fung, P. V. Kamat, *Journal of the American Chemical Society*, 2014, **136**, 758-764, doi: 10.1021/ja411014k.

[8] W. Sun, Y. Li, S. Ye, H. Rao, W. Yan, H. Peng, Y. Li, Z. Liu, S. Wang, Z. Chen, L. Xiao, Z. Bian, C. Huang, *Nanoscale*, 2016, **8**, 10806-10813, doi: 10.1039/c6nr01927g.

[9] C. Zuo, L. Ding, *Small*, 2015, **11**, 5528-5532, doi: 10.1002/smll.201501330.

[10] P. Qin, S. Tanaka, S. Ito, N. Tetreault, K. Manabe, H. Nishino, M. K. Nazeeruddin, M. Grätzel, *Nature Communications*, 2014, **5**, 3834, doi: 10.1038/ncomms4834.

[11] M. D. Irwin, D. B. Buchholz, A. W. Hains, R. P. H. Chang, T. J. Marks, *Proceedings of the National Academy of Sciences of the United States of America*, 2008, **105**, 2783-2787, doi: 10.1073/pnas.0711990105.

[12] H. Abdy, A. Aletayeb, M. Kolahdouz, E. A. Soleimani, *AIP Advances*, 2019, **9**, 015216, doi: 10.1063/1.5063475.

[13] J. Y. Jeng, K. C. Chen, T. Y. Chiang, P. Y. Lin, T. D. Tsai, Y. C. Chang, T. F. Guo, P. Chen, T. C. Wen, Y. J. Hsu, *Advanced Materials*, 2014, **26**, 4107-4113, doi: 10.1002/adma.201306217.

[14] J. Cui, F. Meng, H. Zhang, K. Cao, H. Yuan, Y. Cheng, F. Huang, M. Wang, *ACS Applied Materials & Interfaces*, 2014, **6**, 22862-22870, doi: 10.1021/am507108u.

[15] H. Kim, S. Yang, S.-H. Ahn, C. S. Lee, *Thin Solid Films*, 2016, **600**, 109-118, doi: 10.1016/j.tsf.2016.01.031.

[16] C. Hu, K. Chu, Y. Zhao, W. Y. Teoh, *ACS Applied Materials & Interfaces*, 2014, **6**, 18558-18568, doi: 10.1021/am507138b.

[17] Z. Liu, A. Zhu, F. Cai, L. Tao, Y. Zhou, Z. Zhao, Q. Chen, Y. B. Cheng, H. Zhou, *Journal of Materials Chemistry A*, 2017, **5**, 6597-6605, doi: 10.1039/c7ta01593c.

[18] L. A. García-Cerda, L. E. Romo-Mendoza, M. A. Quevedo-López, *Journal of Materials Science*, 2009, **44**, 4553-4556, doi: 10.1007/s10853-009-3690-6.

[19] X. Xie, C. Gao, X. Du, G. Zhu, W. Xie, P. Liu, Z. Tang, *Materials*, 2018, **11**, 760, doi: 10.3390/ma11050760.

[20] D. Di Girolamo, F. Di Giacomo, F. Matteocci, A. G. Marrani, D. Dini, A. Abate, *Chemical Science*, 2020, **11**, 7746-7759, doi: 10.1039/d0sc02859b.

[21] M. B. Islam, M. Yanagida, Y. Shirai, Y. Nabetani, K. Miyano, *ACS Omega*, 2017, **2**, 2291-2299, doi: 10.1021/acsomega.7b00538.

[22] X. Liu, H. W. Qiao, M. Chen, B. Ge, S. Yang, Y. Hou, H. G. Yang, *Materials Chemistry Frontiers*, 2021, **5**, 3614-3620, doi: 10.1039/d0qm01064b.

[23] J. Asare, D. M. Sanni, B. Agyei-Tuffour, E. Agede, O. K.

Oyewole, A. S. Yerramilli, N. Y. Doumon, *Energies*, 2021, **14**, 1949, doi: 10.3390/en14071949.
[24] J. H. Im, H. S. Kim, N. G. Park, *APL Materials*, 2014, **2**, 081510, doi: 10.1063/1.4891275.
[25] J. Tirado, M. Vásquez-Montoya, C. Roldán-Carmona, M. Ralaiarisoa, N. Koch, M. K. Nazeeruddin, F. Jaramillo, *ACS Applied Energy Materials*, 2019, **2**, 4890-4899, doi: 10.1021/acsaem.9b00603.
[26] Rahul, P. K. Singh, R. Singh, V. Singh, S. K. Tomar, B. Bhattacharya, Z. H. Khan, *Materials Research Bulletin*, 2017, **89**, 292-296, doi: 10.1016/j.materresbull.2017.01.035.
[27] K. Surana, N. A. Jadhav, P. K. Singh, B. Bhattacharya, *Applied Nanoscience*, 2018, **8**, 2065-2069, doi: 10.1007/s13204-018-0887-5.
[28] U. Ashraf, B. Khan, *International Journal of Science and Research*, 2013, **4**, 2405-2408.
[29] N. N. M. Zorkipli, N. H. M. Kaus, A. A. Mohamad, *Procedia Chemistry*, 2016, **19**, 626-631, doi: 10.1016/j.proche.2016.03.062.
[30] M. Srivastava, P. Kumar Singh, B. Gultekin, R. Chandra Singh, *Materials Today: Proceedings*, 2021, **34**, 748-751, doi: 10.1016/j.matpr.2020.04.688.
[31] N. G. Park, K. Kim, *Physica Status Solidi (a)*, 2008, **205**, 1895-1904, doi: 10.1002/pssa.200778938.
[32] N. G. Park, M. Grätzel, T. Miyasaka, K. Zhu, K. Emery, *Nature Energy*, 2016, **1**, 16152, doi: 10.1038/nenergy.2016.152.
[33] A. Mishra, Z. Ahmad, F. Touati, R. A. Shakoor, M. K. Nazeeruddin, *RSC Advances*, 2019, **9**, 11589-11594, doi: 10.1039/c9ra00200f.
[34] A. Peter Amalathas, M. Alkaisi, *Micromachines*, 2019, **10**, 619, doi: 10.3390/mi10090619.
[35] Y. R. Lin, H. P. Wang, C. A. Lin, J. H. He, *Journal of Applied Physics*, 2009, **106**, 114310, doi: 10.1063/1.3267147.
[36] N. Rajamanickam, S. Kumari, V. K. Vendra, B. W. Lavery, J. Spurgeon, T. Druffel, M. K. Sunkara, *Nanotechnology*, 2016, **27**, 235404, doi: 10.1088/0957-4484/27/23/235404.
[37] T. Baikie, Y. Fang, J. M. Kadro, M. Schreyer, F. Wei, S. G. Mhaisalkar, M. Graetzel, T. J. White, *Journal of Materials Chemistry A*, 2013, **1**, 5628, doi: 10.1039/c3ta10518k.
[38] Y. Xu, Synthesis and characterization of silica coated CdSe/CdS core/shell quantum dots, *Virginia Tech*, 2005.
[39] M. El-Kemary, N. Nagy, I. El-Mehasseb, *Materials Science in Semiconductor Processing*, 2013, **16**, 1747-1752, doi: 10.1016/j.mssp.2013.05.018.
[40] D. Mohammadyani, S. A. Hosseini, S. K. Sadrnezhaad, *International Journal of Modern Physics: Conference Series*, 2012, **5**, 270-276, doi: 10.1142/s2010194512002127.
[41] H. Yan, D. Zhang, J. Xu, Y. Lu, Y. Liu, K. Qiu, Y. Zhang, Y. Luo, *Nanoscale Research Letters*, 2014, **9**, 424, doi: 10.1186/1556-276X-9-424.
[42] G.-W. Kim, D. V. Shinde, T. Park, *RSC Advances*, 2015, **5**, 99356-99360, doi: 10.1039/c5ra18648j.
[43] W. Sun, K.-L. Choy, M. Wang, *Molecules*, 2019, **24**, 3466, doi: 10.3390/molecules24193466.
[44] P. Vivo, J. Salunke, A. Priimagi, *Materials*, 2017, **10**, 1087, doi: 10.3390/ma10091087.
[45] X. Xu, Z. Liu, Z. Zuo, M. Zhang, Z. Zhao, Y. Shen, H. Zhou, Q. Chen, Y. Yang, M. Wang, *Nano Letters*, 2015, **15**, 2402—2408, doi: 10.1021/nl504701y.
[46] K. Surana, S. Konwar, P. K. Singh, B. Bhattacharya, *Journal of Alloys and Compounds*, 2019, **788**, 672-676, doi: 10.1016/j.jallcom.2019.02.287.
[47] K. Surana, R. M. Mehra, B. Bhattacharya, *Optical Materials*, 2020, **107**, 110092, doi: 10.1016/j.optmat.2020.110092.

Author Information

Dr. Monika Srivastava *received her PhD in physics from, School of Basic Sciences and Research, Sharda University, Greater Noida, India. During her PhD, her research work was focused on the fabrication of methyl ammonium lead iodide perovskite solar cells in room ambient condition. She is currently working on all inorganic perovskite solar cells.*

Dr. Karan Surana *is currently a UGC-Dr. D.S. Kothari Post Doctoral Fellow (DSKPDF) at Sardar Patel University, Gujarat. He received his Ph.D in Nanoscience and Technology from Sharda University, Greater Noida in 2020. During Ph.D he worked on the modification of the working electrode of Quantum dot solar cells.*

Dr. Pramod Kumar Singh*, HoD of Physics and Environment, SBSR, Ph.D. from Banaras Hindu University (BHU), India is currently working as Professor, Department of Physics, School of Basic Sciences and Research, Sharda University. He is involved in research within research specialized area like Polymer Electrolyte, Nanoporous materials for energy devices, Dye sensitized solar cell, Supercapacitors.*

Dr. R. C. Singh *has rich experience of more than 30 years as a researcher out of which more than 10 years as Professor of Physics. Presently, Dr. Singh is Professor of Physics and in addition to that he is also Controller of Examinations of Sharda University. His area of research interest includes study of phase transitions in molecular liquids using density-functional theory; Time-series analysis using wavelets; Biometrics and Solar cells.*